## PAPER

Check for updates

# Revealing the mechanism of synergistic antibacterial effect of silver nanoparticles in combination with vancomycin against *Enterococcus* species by fluorescence microscopy visualization

Lucie Válková,[†ab] Lucie Suchánková Hochvaldová,[†a] Martin Mistrík,[c] Milan Kolář,[d] Kateřina Langová,[b] Hana Kolářová,[b] Barbora Štefková,[a] Robert Prucek, [a] Libor Kvítek [a] and Aleš Panáček [*a]

Silver nanoparticles (Ag NPs) significantly enhance the antibacterial activity of antibiotics and even restore their effect against resistant strains, making them a promising option for overcoming bacterial resistance to antibiotics. However, the exact mechanism of their synergistic effect with antibiotics at the cellular level has not been elucidated. In this work, we synthesised rhodamine-labelled Ag NPs and described, for the first time, the multi-level non-specific mechanism of the synergistic antibacterial effect of fluorescently labelled Ag NPs and a fluorescent vancomycin conjugate against vancomycin-resistant enterococci using high-resolution fluorescence microscopy. The multi-level mechanism of the synergistic effect of Ag NPs and vancomycin is mainly based on the disruption of the strength and integrity of the cell wall, which becomes unstable, loses strength and subsequently disintegrates due to the oxidative stress caused by Ag NPs and the residual effect of vancomycin. In addition, Ag NPs penetrate the bacterial cell and deform the bacterial DNA, which also significantly increases the synergistic antibacterial effect. This work represents an advance in understanding the mechanism of synergistic effect of Ag NPs with antibiotics against resistant bacteria, an important finding for a potential approach to effectively combat the unsolved problem of increasing resistance of pathogenic bacteria to traditional antibiotics.

## 1. Introduction

After their introduction, the misuse and overuse of antibiotics led to the rapid emergence of bacterial resistance to antibiotics. The emergence of antibiotic-resistant bacteria, or 'superbugs', poses a global public health threat due to their resistance to our most effective last-line antibiotics.[1] Highly resistant bacteria causing very difficult-to-treat infections currently include enterococci such as *Enterococcus faecium* and *Enterococcus faecalis*, which show resistance to multiple antibiotics with different mechanisms of action.[2,3] Infections caused by resistant enterococci often affect the intra-abdominal area, urinary tract, bloodstream, post-surgical areas and vascular catheter area, especially in immuno-compromised or seriously ill patients in hospital care. The mortality rate in patients with bloodstream infections caused by resistant enterococci can be as high as 70%, and approximately half of these deaths can be attributed directly to this infection.[2] The glycopeptide antibiotic vancomycin, whose mechanism of action is to inhibit the biosynthesis of the bacterial cell wall of Gram-positive bacteria, is used to treat infections caused by resistant enterococci.[4] The antibacterial efficacy of vancomycin is dependent on the stage of the bacterial cell cycle, as inhibition of cell wall synthesis occurs at the site of the bacterial dividing septum – *i.e.* at the site where cell wall synthesis occurs during the cell division process.[5,6] The resistance mechanism to vancomycin found in *Enterococcus* species involves the alteration of the peptidoglycan synthesis pathway. The D-alanyl-D-lactate variation results in the loss of one hydrogen-bonding interaction (four, as opposed to

[a] *Department of Physical Chemistry, Faculty of Science, Palacký University, 17. listopadu 1192/12, Olomouc 779 00, Czech Republic.*
*E-mail: ales.panacek@upol.cz; Fax: +420585634425; Tel: +420585634427*
[b] *Department of Medical Biophysics, Faculty of Medicine and Dentistry, Palacký University, Hněvotínská 3, Olomouc 77900, Czech Republic*
[c] *Institute of Molecular and Translational Medicine, Faculty of Medicine and Dentistry, Palacký University and University Hospital in Olomouc, Hněvotínská 1333/5, Olomouc 779 00, Czech Republic*
[d] *Department of Microbiology, Faculty of Medicine and Dentistry, Palacký University, Hněvotínská 3, Olomouc 77900, Czech Republic*
† Equally contributing authors.

This journal is © The Royal Society of Chemistry 2025

*J. Mater. Chem. B*, 2025, **13**, 10903–10915 | **10903**

five for D-alanyl-D-alanine) being possible between vancomycin and the peptide. The D-alanyl-D-serine variation causes a six-fold loss of affinity between vancomycin and the peptide, likely due to steric hindrance. The presence of such bacterial resistance under *in vitro* conditions leads to an increase in the minimum inhibitory concentration (MIC) of the antibiotic to more than 64 mg L$^{-1}$, which is well above clinically achievable therapeutic concentrations.[7–9] Another mechanism of bacterial resistance to vancomycin in Gram-positive strains is the increased tendency of vancomycin to bind to false target sites in the cell wall, which prevents the antibiotic from acting at the site of the dividing septum.[6,10]

An option to overcome bacterial resistance could be to restore the antibacterial effect of antibiotics by combining them with novel nanostructured antibacterial agents, *e.g.* silver nanoparticles (Ag NPs), which themselves exhibit high anti-bacterial activity against susceptible and multidrug-resistant bacteria and, in combination with antibiotics, very effectively restore their antibacterial activity against resistant bacteria.[11,12] Ag NPs exhibit high antibacterial efficacy, partly because their mechanism of action is multilevel, unlike antibiotics.[13] For example, Ag NPs are able to anchor themselves to the cell wall of bacteria and subsequently disrupt it. They then cause structural changes in the cytoplasmic membrane, eventually leading to the death of the entire cell. Another possible mechanism of antibacterial action is the release of silver ions, which subsequently interact with the thiol groups of many proteins and enzymes and are able to inactivate them.[14] When Ag NPs penetrate inside a microbial cell, they can interact with cellular structures and biomolecules such as proteins, lipids and DNA. In particular, interactions with ribosomes lead to their denaturation, causing inhibition of translation and protein synthesis.[15] Ag NPs also cause the formation of reactive oxygen species (ROS) such as superoxide anion radicals, hydroxyl radicals and hydrogen peroxide. ROS in elevated concentrations can react directly with membrane lipids, proteins and DNA in bacterial cells and lead to oxidative stress and subsequent cell death.[16]

In contrast to the precisely described mechanism of action of antibiotics and the widely described mechanism of action of Ag NPs, the mechanism of synergistic action of antibiotics and Ag NPs has not been deeply and extensively investigated. In addition, the mechanism of synergistic action and the principle of restoration of antibiotic action in combination with Ag NPs may vary depending on the mechanism of action of the antibiotic and the resistance mechanism of the bacterium.[17,18] For example, Ag NPs may facilitate the penetration of antibiotics into the bacterium by changing the permeability of the cytoplasmic membrane or may interact with each other when the cell wall is disrupted.[19,20] Furthermore, Ag NPs may inhibit the formation of bacterial biofilms, which are closely linked to bacterial resistance to antibiotics.[21,22] The antibacterial mechanism involved in synergism may further involve the production of hydroxyl radicals and it is also associated with an ATP-dependent function such as the multi-drug resistance pumps, leading to a reduction in bacterial viability and ultimately a reduction in the MIC of antibiotics.[19]

The mechanism of synergy can also be explained by the binding interaction between the antibiotic and the nanoparticle. In this case, the amino and hydroxyl groups of the antibiotics are bound to the Ag NPs by chelation, leading to the formation of a conjugate in which the silver core is surrounded by antibiotic molecules. The nanoparticles are then selectively attracted to the bacterial surface consisting of glycoproteins and phospholipids, thus acting as drug carriers that transport the antibiotics near the cytoplasmic membrane. This results in increased contact with the membrane and an increase in the concentration of antibiotics in its vicinity. For example, Deng *et al.* reported that the presence of tetracycline increases bacterial binding of silver by 21% and enhances Ag$^+$ release by 26%.[23] Membrane permeability can also be increased by binding Ag NPs to sulfur-containing proteins, which improves the infiltration of the antibiotic into the cell.[22,24,25]

In the case of the combination of Ag NPs with vancomycin, *in vitro* and *in vivo* synergistic effects against both Gram-positive and Gram-negative bacteria have been studied and described in many papers, where they are effective against a wide range of resistant bacterial strains.[26–40] However, the mechanism of the synergistic antibacterial effect of vancomycin in combination with Ag NPs has not yet been studied and confirmed, *i.e.*, the mechanism of restoration of the antibacterial effect of vancomycin in combination with Ag NPs against vancomycin-resistant bacteria has not yet been described.

In this work, we present the elucidation of the mechanism of synergistic effect of Ag NPs and the glycopeptide antibiotic vancomycin against vancomycin-susceptible *E. faecalis* and vancomycin-resistant *E. faecium* by fluorescence microscopy. For this purpose, 10 nm Ag NPs fluorescently labelled with rhodamine-B-isothiocyanate (RBITC) were synthesized and combined with fluorescein labelled vancomycin. For the first time, this work elucidated the mechanism of synergistic antibacterial action and recovery of vancomycin in combination with Ag NPs against vancomycin-resistant *E. faecium* based on their localization in bacterial cells by fluorescence microscopy.

## 2. Methods

### 2.1. Chemicals and biological materials

Silver nitrate (Fagron, p.a.), ammonium hydroxide (Sigma-Aldrich, 28–30% aqueous solution, p.a.), sodium hydroxide (Lach-Ner, p.a.), sodium salt of polyacrylic acid (Sigma-Aldrich, MW 15 000, 35 wt%) and sodium tetrahydridoborate (Sigma-Aldrich, ≥98%), and rhodamine B isothiocyanate (Sigma-Aldrich, p.a.). Vancomycin (Sigma-Aldrich, p.a.) and fluorescent BODIPY™ FL vancomycin conjugate (Thermo Fisher Scientific, p.a.) were used to study the synergistic effects of Ag NPs. Vancomycin-susceptible *E. faecalis* CCM 4224 (VSE) obtained from the Czech Collection of Micro-organisms (Masaryk University, Brno) and vancomycin-resistant *E. faecium* 419 (VRE) obtained from the microorganism collection of the Department of Microbiology at the Faculty of Medicine of Palacký University in Olomouc were used synergistic antibacterial determinations. Mueller–Hinton (MH) broth was used to culture the bacteria. Phosphate buffer was used to wash the bacteria

10904 | *J. Mater. Chem. B*, 2025, **13**, 10903–10915

This journal is © The Royal Society of Chemistry 2025

(0.1 mol dm$^{-3}$, pH = 7.4). Tested bacteria were stained with 4′,6-diamidino-2-phenylindole (DAPI) (Thermo Fisher Scientific) to visualize the cell nucleus using vectashield mounting reagent (Vector Laboratories, Inc.). A fluorescent probe CM-H$_2$DCFDA (Invitrogen™), phosphate buffer and hydrogen peroxide solution (Sigma-Aldrich, 30% (w/w) in H$_2$O) were used for the determination of reactive oxygen species.

## 2.2. Synthesis and characterization of fluorescently labelled Ag NPs

Ag NPs were synthesized using the modified Tollens method by reducing the soluble complex compound [Ag(NH$_3$)$_2$]$^+$ with NaBH$_4$ as a reducing agent and sodium polyacrylate as a stabilizer. Rhodamine B isothiocyanate was used as a fluorescent marker. The synthesis took place at room temperature with vigorous stirring on an electromagnetic stir plate according to the following procedure: 5 ml of silver nitrate solution (5 × 10$^{-3}$ mol dm$^{-3}$) was mixed with 0.6 ml of ammonium hydroxide (0.1 mol dm$^{-3}$), 11.9 ml of H$_2$O, 2.5 ml of 0.5% solution of sodium polyacrylate, and finally, 5 ml of sodium borohydride solution (10$^{-2}$ mol dm$^{-3}$). Reduction of silver cations occurred immediately after the addition of sodium borohydride, changing the dispersion from clear to honey-brown. Subsequently, 19.8 ml of the prepared Ag NPs dispersion was taken, and 0.2 ml of RBITC solution with a concentration of 0.75 × 10$^{-2}$ mol dm$^{-3}$ was added. The mixture was incubated for 1 hour on a roller mixer to allow the dye to bind to the surface of the nanoparticles. After incubation, the labelled Ag NPs were purified using dialysis with a spectra dialysis membrane with a molecular weight cutoff of 50 kDa. These prepared nanoparticles are referred to as Ag-RBITC in the text. After purification, the size and zeta potential of the labelled Ag-RBITC particles were measured using dynamic light scattering and electrophoretic mobility methods on a Zetasizer Nano ZS instrument (Malvern, UK). The size and morphology of the Ag-RBITC particles were characterized using transmission electron microscopy on a JEM 2010 instrument (Jeol, Japan). Absorption spectra of a 10 times diluted dispersion of Ag NPs, Ag-RBITC NPs before and after dialysis and solution of RBITC dye (the concentrations of Ag and RBITC were equivalent in all the samples) were recorded using a Specord S 600 instrument (Analytik Jena, Germany). After purification, the silver concentration in the dispersion of Ag-RBITC particles was determined using atomic absorption spectroscopy on a ContraAA 300 instrument (Analytik Jena, Germany). For AAS, Ag NPs were mineralized using 2% nitric acid. Furthermore, the Ag-RBITC particles were characterized using Raman spectroscopy on a DXR Raman microscope (ThermoFisher Scientific), and their excitation and emission maps were measured using a fluorescence spectrometer FLS980 (Edinburgh Instruments, United Kingdom). Prior to Raman spectroscopy measurements, the Ag-RBITC particles were aggregated with Mg$^{2+}$ ions by adding 0.2 ml of a 1 mol dm$^{-3}$ solution of Mg(NO$_3$)$_2$·6H$_2$O to a 2 ml dispersion of Ag NPs, followed by separation using centrifugation at 15 000 rpm for 15 minutes. The samples were then washed twice with distilled water and centrifuged. After washing, the sample was dried in a vacuum dryer (40 °C, 300 mbar).

## 2.3. Antibacterial assay

A standard microdilution checkerboard method using cation-adjusted MH broth was used (according to standard testing CLSI and EUCAST protocols) to determine the individual and joint effect of the vancomycin and Ag NPs. For each antimicrobial assay, a fresh bacterial suspension was prepared from bacteria that had been grown on blood agar at 35 °C for 24 h. The optical density of the bacterial inoculum was determined to be equal to 1 based on McFarland's standard using a densitometer (Densi-La-Meter, LACHEMA, Czech Republic); after appropriate dilution, this gave a starting concentration of 5 × 10$^6$ CFU per ml for microbial testing. To determine combined effect, twofold dilutions of each drug was used to test the different combinations. Growth control wells containing the medium were included in each plate. Ag NPs and Ag-RBITC particles were tested in concentration range: 27; 13.5; 6.75; 3.375; 1.688; 0.844; 0.422; 0.211; 0.105; 0.053; 0.06 and 0 mg L$^{-1}$ (diluted horizontally on the 96-well plate), while vancomycin concentration values were: 512; 256; 128; 64; 32; 16; 8 and 0 mg L$^{-1}$ for vancomycin-resistant *E. faecium* (VRE) and 4; 2; 1; 0.5; 0.25; 0.125; 0.0625 and 0 mg L$^{-1}$ for vancomycin-susceptible *E. faecalis* (VSE) (diluted vertically on the 96-well plate). To determine the enhancement of antibacterial activity resulting from combined treatment with Ag NPs and Ag-RBITC nanoparticles combined with vancomycin, 96-well microtitration plates were filled with vertically diluted vancomycin and horizontally diluted silver NPs. Afterwards, plates were inoculated by bacteria to final amount 5 × 10$^6$ bacteria per well. Final volume of the well was 100 μL. The microtitration plate was incubated at 35 °C for 24 h and the inhibitory concentrations of the substances alone and in combinations were determined as the lowest concentration of antibacterial agent that visibly inhibited bacterial growth. The fractional inhibitory concentration (FIC) index was calculated using the following equation:

$$FIC = \frac{MIC_{AgNPs} \text{ in combination}}{MIC_{AgNPs} \text{ alone}} + \frac{MIC_{ATB} \text{ in combination}}{MIC_{ATB} \text{ alone}}$$

Results are reported as average FIC values (calculations shown in SI); antibacterial effects are classified as synergistic (FIC ≤ 0.5), partially synergetic (0.5 < FIC ≤ 1), additive (FIC = 1), indifferent (1 < FIC < 4), or antagonistic (FIC ≥ 4).[41–43]

## 2.4. Fluorescence microscopy of bacteria exposed to Ag-RBITC nanoparticles and vancomycin

The localization and mechanism of action of fluorescently labelled Ag NPs and vancomycin in bacterial cells were visualized and investigated against vancomycin-susceptible *E. faecalis* (VSE) and vancomycin-resistant *E. faecium* (VRE) using laser scanning confocal fluorescence microscopy and the super-resolution SIM technique (Zeiss Axioimager Z.1 platform equipped with an LSM780 module for confocal laser scanning microscopy). Bacteria were first inoculated onto blood agar and cultured at

This journal is © The Royal Society of Chemistry 2025

*J. Mater. Chem. B*, 2025, **13**, 10903–10915 | **10905**

35 °C for 24 hours. The grown bacteria were then used to prepare a bacterial suspension in saline buffer, where the number of bacteria was determined by optical density (Densi-La-Meter; LACHEMA, Czech Republic) to a McFarland 1 value corresponding to a bacterial count of $5 \times 10^8$ CFU per ml. Subsequently, 2 ml of bacterial suspension was collected in a tube and supplemented with 18 ml of MH broth. The tube with the bacterial suspension was placed in a thermostat and incubated for 6 h at 35 °C when the bacteria reached the mid-exponential growth phase. At this growth phase, the bacteria were collected and used to prepare experimental samples containing labelled Ag-RBITC nanoparticles, vancomycin and a combination of vancomycin and Ag-RBITC nanoparticles. Dispersions of Ag-RBITC nanoparticles and solution of unlabelled vancomycin (standard antibiotic) with fluorescently labelled vancomycin (vancomycin BODIPY FL) at 1:1 molar ratio were used to prepare the experimental samples. Experimental samples were prepared as follows: 0.4 ml of VSE or VRE bacterial suspension collected in the mid-exponential phase was added to Eppendorf tube, to which a dispersion of fluorescently labelled Ag-RBITC nanoparticles and a solution of fluorescently labelled vancomycin and a mixture of fluorescently labelled vancomycin and labelled Ag-RBITC nanoparticles were subsequently added, respectively. The Eppendorfs were then filled with distilled water to a final volume of 1 ml. The final concentrations of the tested substances in each sample were as follows: 10 mg $L^{-1}$ of Ag in Ag-RBITC sample; 1 mg $L^{-1}$ of vancomycin in mixture of vancomycin and vancomycin BODIPY FL; 1 mg $L^{-1}$ of vancomycin and 10 mg $L^{-1}$ of Ag NPs in sample of mixture of vancomycin together with Ag-RBITC. Thus, a total of 6 samples of suspensions of vancomycin susceptible and resistant bacteria exposed to labelled Ag-RBITC, RBITC, vancomycin and their combination were prepared. The prepared samples are then referred to as follows in the text: VSE$_{Ag}$ and VRE$_{Ag}$ – susceptible and resistant strain exposed to 10 mg $L^{-1}$ of labelled silver NPs; VSE$_{Van}$ and VRE$_{Van}$ – susceptible and resistant strain exposed to 1 mg $L^{-1}$ of vancomycin (mixture of non-labelled and labelled vancomycin in a 1:1 ratio); VSE$_{Van\_Ag}$ and VRE$_{Van\_Ag}$ – susceptible and resistant strain exposed to a mixture of 1 mg $L^{-1}$ of vancomycin and 10 mg $L^{-1}$ of Ag NPs. After preparation, samples were incubated for 15 min at 25 °C on a rotary mixer. Subsequently, bacteria were purified by centrifugation (3500 rpm), washed twice with phosphate-buffered saline (PBS) ($c = 0.1$ mol dm$^{-3}$, pH = 7.4) and twice with distilled water. After washing, the bacteria were resuspended in 50 µl of water and plated on a microscope slide and allowed to dry in a vacuum oven (40 °C, 300 mba). After drying, the bacteria were fixed on the microscope slide by passing the non-luminous part of the flame three times. The samples of the bacteria thus prepared and fixed on the microscope slide were used for fluorescence microscopy. Prior to microscopic observation, bacterial DNA was stained with 4,6-diamidino-2-phenylindole (DAPI) solution at concentration 0.002 mg $L^{-1}$, and the slide was incubated with DAPI for 30 min in the dark at room temperature. Vectashield mounting agent was used to fix the coverslip.

### 2.5. ROS determination

Production and quantification of reactive oxygen species (ROS) was performed by recording the fluorescence intensity of the CM-H2DCFDA probe (Invitrogen by Thermo Fisher Scientific, Waltham, MA, USA) in a microtiter plate using microplate reader Synergy HT (BioTek® Instruments, Inc. Winooski, Vermont USA). During an incubation inside cells, CM-H2DCFDA is reduced to colourless CM-H2DCF by intracellular esterases and thiols. Due to the presence of ROS it is oxidized to form green fluorescent chloroform dichlor fluorescein (DCF). The bacteria were first preincubated on blood agar for 24 h. Subsequently, a bacterial suspension containing $5 \times 10^8$ CFU per ml of bacteria in saline was prepared (1 McFarland, determined using optical densitometer (Densi-La-Meter® Erba Lachema, Czech Republic)). ROS production was analysed for Ag NPs and vancomycin alone and for their combination. Ag NPs alone were tested at concentrations of 5; 10; 20; 30; 40 and 50 mg $L^{-1}$, vancomycin at 1 mg $L^{-1}$ and the combination at 1 mg $L^{-1}$ vancomycin and 10 mg $L^{-1}$ Ag NPs. The working concentration of the CM-H2DCFDA probe in all samples was 5 µM. After the addition of Ag NPs, vancomycin, their combination, and the CM-H2DCFDA probe at their respective concentrations, bacteria at a concentration of $5 \times 10^6$ CFU per ml were subsequently injected into the wells of the 96-well culture plate, which were then filled to a final volume of 100 µL. The plate was then covered with cellophane film and placed in a plate reader. The fluorescence intensity of the probe was recorded at 30 min intervals using a 485 nm excitation filter and a 540 nm emission filter for 24 h. The value of the relative fluorescence unit is directly proportional to the H$_2$O$_2$ concentration; therefore it directly reflects the increase and change in the amount of ROS present. All experiments were performed in triplicate, and the standard deviation ± SD of three independent experiments was calculated. A hydrogen peroxide solution of 5; 10; and 80 mM was used as a positive control in the presence and absence of bacteria, respectively. ROS production was also measured in negative controls containing the test substances without the presence of bacteria, where the original volume of bacterial suspension in the samples was replaced by PBS. Another negative control was a bacteria-free sample containing Ag NPs, vancomycin and their combination.

### 2.6. Statistics and reproducibility

All tests were performed at a significance level of 0.05. If the $p$-value was less than 0.05, the differences were considered statistically significant and are indicated by asterisks. IBM SPSS Statistics for Windows, Version 23.0 statistical software was used for statistical processing (Armonk, NY: IBM Corp.).

## 3. Results and discussion

### 3.1. Synthesis and characterization of fluorescently labelled Ag NPs

For the synthesis of Ag NPs, a modified Tollens process consisting in the reduction of the silver ammonia complex with a suitable reducing agent was used. In this case, the strong

10906 | J. Mater. Chem. B, 2025, **13**, 10903–10915

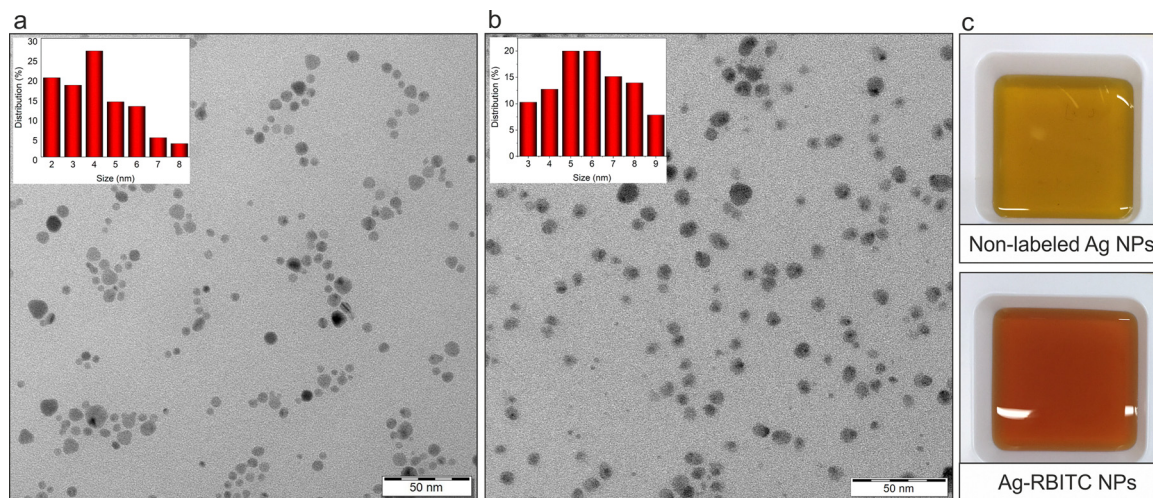This journal is © The Royal Society of Chemistry 2025

Fig. 1 TEM image of (a) non-labelled Ag NPs, (b) RBITC-labelled Ag NPs, and image of (c) light-yellow colour of dispersion of non-labelled Ag NPs (upper picture) and dark-yellow colour of dispersion of RBITC labelled Ag NPs (lower picture).

reducing agent $NaBH_4$ was used, allowing the synthesis of relatively small Ag NPs (Fig. 1). The size of the synthesized non-labelled (as prepared) as well as rhodamine-labelled Ag NPs (Ag-RBITC) after purification of the dispersion by dialysis was determined by dynamic light scattering (DLS) and transmission electron microscopy (TEM). In the case of DLS, the average size was 10.1 nm ± 3 nm and 10.8 nm ± 3 nm (includes the hydrodynamic average), respectively which is confirmed by the TEM images (Fig. 1a and b), showing spherical Ag particles with an average size of 4 nm (non-labelled Ag NPs) and 6 nm (Ag-RBITC) with a relatively narrow size distribution of 2–8 nm and 3–9 nm (does not include the hydrodynamic average), respectively. The silver concentration in the dispersion after purification of the Ag-RBITC dispersion was determined by atomic absorption spectroscopy (AAS) and was 57.6 mg $L^{-1}$. The presence of RBITC fluorescent dye bound to the Ag NPs is already evident from the coloration of the dispersion, which shows a darker yellow coloration in contrast to the yellow coloration of the Ag NPs dispersion without bound RBITC dye (Fig. 1b).

**3.1.1. Absorption spectroscopy.** The change in the colour of the dispersions of Ag NPs without dye and Ag-RBITC NPs with dye and simultaneously the presence of RBITC dye bound to Ag NPs in the Ag-RBITC particle sample after purification was monitored by, among others, absorption spectroscopy (Fig. 2). The absorption peak of the surface plasmon of non-labelled Ag NPs is in the region of 400 nm (gray curve). After the dye was bound to Ag NPs, the peak of Ag NPs was broadened and shifted to longer wavelengths (red curve). This shift is due to the change in the chemical environment and the change in the chemical composition on the surface of the Ag NPs due to the binding and presence of RBITC molecules. Also, after the binding of the RBITC dye, there was a decrease in the surface plasmon absorbance of the Ag NPs due to the decrease in the concentration of Ag NPs caused by their adsorption on the walls of the plastic tube during incubation on the rotary shaker.
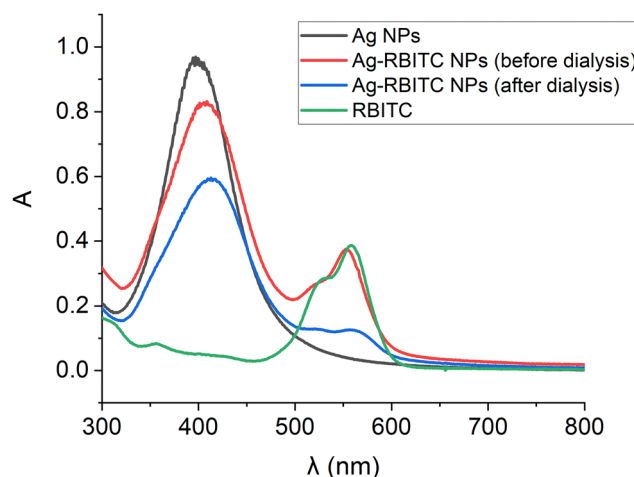


Fig. 2 Absorption spectra of non-labelled Ag NPs (grey), labelled Ag-RBITC NPs before (red) and after dialysis (blue), and RBITC itself (green).

The peak in the range 500–600 nm on the red curve belongs to the RBITC dye present in the Ag-RBITC particle dispersion before purification (bound and unbound dye together), whose absorption maximum is located at 555 nm and remained unchanged in comparison to the absorption maximum of the RBITC dye itself (green). Based on this comparison, it is clear that the peak belonging to the pure RBITC dye was also recorded in the spectrum of Ag-RBITC particles before and after purification by dialysis, confirming the successful functionalization of the Ag NP surface with the RBITC dye. After purification by dialysis, which was performed to remove the unbound fluorescent dye, the absorbance of both the RBITC dye and the Ag NPs decreased (blue curve), which was due to the removal of the unbound dye and the decrease in the concentration of Ag NPs in the sample, respectively, which adsorbed to the inner wall of the dialysis membrane during dialysis.

This journal is © The Royal Society of Chemistry 2025

J. Mater. Chem. B, 2025, 13, 10903–10915 | 10907

**3.1.2. Fluorescence spectroscopy.** To further verify the presence of the fluorescent dye RBITC bound to Ag NPs, the excitation and emission spectra as well as the spectrum of the RBITC dye itself were measured at a concentration of $10^{-7}$ mol dm$^{-3}$ (Fig. 3). According to the excitation and emission maps of the RBITC dye and Ag-RBITC samples, it can be seen that the range of the excitation (490–580 nm) and emission (550–680 nm) band is the same for the sample of unbound dye and the dye bound to Ag NPs. The emission maxima and overall profile of the RBITC fluorescence remain unchanged upon conjugation with Ag nanoparticles. This suggests that the optical properties of the dye are preserved, and no significant quenching or enhancement occurs.

A plausible explanation lies in the structure of the Ag-RBITC system. The Ag NPs used in this study are stabilized by polyacrylic acid which is added to the reaction mixture at a concentration of 0.5% (w/v) in the presence of 108 mg L$^{-1}$ silver. The PAA molecules are adsorbed onto the Ag NP surface, likely through a combination of electrostatic and covalent interactions, forming a protective and functional interlayer. When RBITC is subsequently introduced, its binding occurs through electrostatic attraction or possible hydrogen bonding with the carboxylic groups of PAA, rather than by direct contact with the metallic silver surface. This interfacial separation between the fluorophore and the metallic core is likely sufficient to prevent both metal-induced quenching (which typically requires sub-nanometer distances) and metal-enhanced fluorescence (which depends on precise plasmon–fluorophore coupling). Therefore, the lack of change in the emission profile is attributed to the spatial and electronic decoupling of the RBITC molecules from the Ag core by the PAA interlayer.

**3.1.3. Raman spectroscopy.** Ag-RBITC were further characterized by Raman spectroscopy to verify the presence of fluorescent dye on the surface of Ag NPs (Fig. 4). The observed Raman peaks, including those at 1641 cm$^{-1}$ (indicating a carbonyl group, C=O), 1528 cm$^{-1}$ (associated with aromatic rings), 1504 cm$^{-1}$ (suggesting double bonds, C=C), and others at 1356 cm$^{-1}$, 1277 cm$^{-1}$, 1197 cm$^{-1}$, 1075 cm$^{-1}$, 782 cm$^{-1}$, and 681 cm$^{-1}$ (potentially related to various functional groups like C–N, C–H, and aromatic ring modes), collectively suggest that the molecule under investigation exhibits vibrational modes
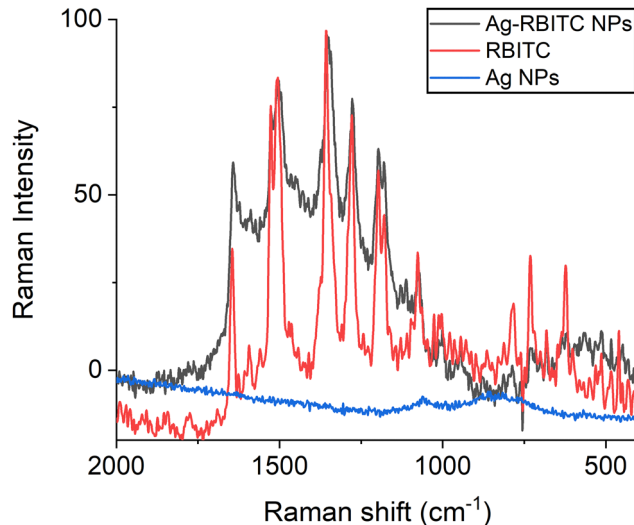


Fig. 4 Raman spectra of RBITC dye (red curve), Ag-RBITC (black curve) particles and non-labelled Ag NPs (blue curve).

and functional groups consistent with RBITC.[44–50] Notably, it is worth mentioning that all the main peaks observed in Fig. 4 in nanoparticles labelled by rhodamine (Ag-RBITC) correspond to the peaks measured for the rhodamine molecule itself (RBITC), strongly indicating the presence of RBITC or a closely related compound. This alignment of Raman peaks with RBITC's characteristic spectral features provides substantial evidence for the presence of RBITC within the labelled nanoparticles (Ag-RBITC). The Raman spectrum of non-labelled Ag NPs stabilized with polyacrylic acid (PAA) displays weak overall intensity, with two low-intensity maxima observed at approximately 850 cm$^{-1}$ and 1060 cm$^{-1}$. These bands may correspond to C–C skeletal vibrations or C–H rocking modes of the aliphatic polymer backbone. Alternatively, given the use of sodium borohydride during nanoparticle synthesis, these signals may arise from B–O or B–H deformation vibrations, which are also typically observed in this spectral region.[44–50] The characteristic C=O or COO$^-$ stretching vibration around 1700 cm$^{-1}$ is not observed, likely due to the coordination of deprotonated carboxylate groups to the silver surface, which can suppress or
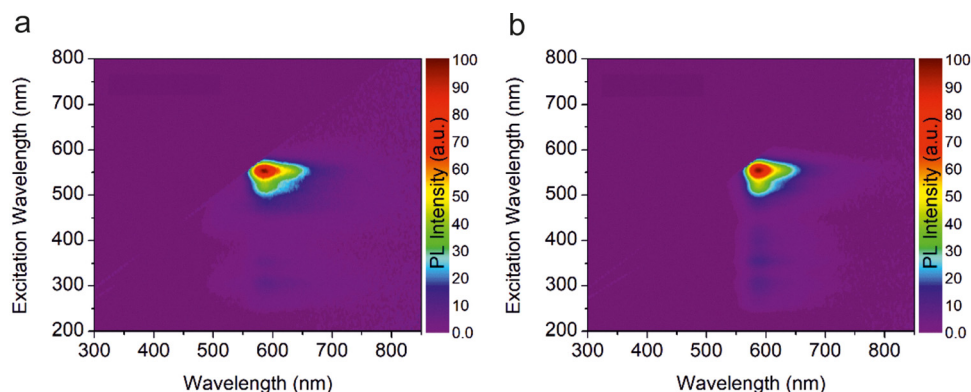


Fig. 3 Excitation and emission map of (a) Ag-RBITC particles and (b) pure RBITC solution.

**10908** | *J. Mater. Chem. B*, 2025, **13**, 10903–10915

This journal is © The Royal Society of Chemistry 2025

shift their Raman response. The low overall Raman intensity is consistent with the intrinsically low scattering efficiency of non-aromatic polymers and may also result from polymer adsorption conformations that limit access to plasmonic hot spots, reducing surface-enhanced Raman scattering efficiency.

## 3.2. Determination of the antibacterial synergistic effect of Ag-RBITC and vancomycin

Prior to the observation of the synergistic effect mechanism by fluorescence microscopy, MICs of Ag-RBITC and Ag NPs nanoparticles alone and vancomycin against vancomycin-susceptible *Enterococcus faecalis* (VSE) and vancomycin-resistant *Enterococcus faecium* (VRE) were determined by dilution method. The synergistic antibacterial effect Ag-RBITC NPs and non-labelled Ag NPs was also quantified by determining their MIC when combined with vancomycin and the fractional inhibitory concentration (FIC) was determined from these values. The resulting MIC values of non-labelled Ag NPs, Ag-RBITC nanoparticles and vancomycin alone and in combination, including FIC values, are shown in Table 1. The Ag-RBITC particles and pure Ag NPs alone showed the same antibacterial effect against both VSE and VRE with the same MIC equal to 13.5 mg $L^{-1}$. However, the MIC of vancomycin was different against VSE and VRE respectively. VSE was inhibited at a concentration of 2 mg $L^{-1}$, while VRE was inhibited at a concentration of 512 mg $L^{-1}$, confirming the resistance to vancomycin. In testing the synergistic antibacterial effect, the maximum synergistic effect was determined at an Ag NPs and Ag-RBITC MIC of 3.38 mg $L^{-1}$ and a vancomycin MIC of 2 mg $L^{-1}$ against VRE, corresponding to an FIC value of 0.25. Against VSE, the maximum synergistic effect was determined at an Ag NPs and Ag-RBITC MIC of 1.69 mg $L^{-1}$ and 1 mg $L^{-1}$ of vancomycin, corresponding to an FIC index of 0.63. Such low FIC values confirm the synergistic antibacterial effect of the combination of non-labelled Ag NPs and Ag-RBITC with vancomycin against both VSE and VRE. It must be emphasized that such low synergistic concentrations of Ag NPs with vancomycin are quite safe and do not present cytotoxicity to mammalian cells, as confirmed by our previous study[51] and also by the newly obtained data in this study. To verify the biocompatibility in this study, human HaCaT keratinocytes were exposed to Ag-RBITC alone and Ag-RBITC in combination with vancomycin in a dose-dependent manner, and then cell viability was tested using the MTT assay. Based on the results obtained, the cell viability of HaCaT cells was not significantly decreased even at the maximum concentration of 40 mg $L^{-1}$ Ag-RBITC (Fig. S1(a)). Similarly, Ag NPs in combination with vancomycin at concentrations exhibiting synergistic antibacterial effects did not affect the viability of the human keratinocyte cell line (Fig. S1(b)).

## 3.3. Fluorescence microscopy of bacterial cells exposed to vancomycin, Ag-RBITC and their combination

With fluorescently labelled Ag NPs and fluorescently labelled vancomycin, their localization as well as the type and mechanism of cellular damage in the bacterial cell could be investigated after 15 min of incubation in VSE and VRE bacteria. The mechanism of the antibacterial action of vancomycin is bactericidal and involves inhibition of cell wall synthesis in the septum.[5,6] Bacteria were therefore allowed to grow to the mid-exponential phase, when septum formation and bacterial division are just occurring. The localization and mechanism of action of fluorescently labelled vancomycin, Ag-RBITC dye in bacterial cells was visualized by laser scanning confocal fluorescence microscopy and the super-resolution structured illumination microscopy (SIM) technique. The green signal in the images corresponds to the fluorescence of vancomycin (BODIPY fluorescent dye), the fluorescence of Ag NPs (RBITC fluorescent dye) is shown in red, and the blue signal shows the fluorescence of 4′,6-diamidino-2-phenylindole (DAPI) stained bacterial DNA.

**3.3.1. VSE and VRE bacteria exposed to vancomycin.** The bactericidal efficacy of vancomycin is dependent on the stage of the bacterial cell cycle, as it acts through the septum.[6] The bacteria were therefore allowed to grow to the mid-exponential phase, when the bacteria are dividing vigorously. Synthesis of the cell wall takes place at the sites of cell division in the form of a flat circular plate, which is subsequently cleaved and transformed to form new hemispherical daughter cell poles.[5] From the images of $VSE_{Van}$ and $VRE_{Van}$ bacteria (Fig. 5a and b) captured by fluorescence microscopy after 15 minutes of incubation with vancomycin, it is evident and obvious that the bacterial DNA was intact and circularly arranged with no obvious deformations in both bacteria, but the distribution of vancomycin in the cell wall is different in these bacteria as expected. In the case of $VSE_{Van}$, as expected, vancomycin was localized in the septum in addition to the cell wall, confirming its positive specific bactericidal effect by binding to target sites in the cell wall and in the formed cell wall in the septum. In contrast, the localization of vancomycin in $VRE_{Van}$ (Fig. 5b) was evident only in the cell wall but not in the septum due to the bacterial resistance mechanism. Thus, in contrast to $VSE_{Van}$, the presence of vancomycin in the septum of $VRE_{Van}$ was not evident, confirming that vancomycin was unable to bind to the target site in the septum due to $VRE_{Van}$ resistance

**Table 1** MIC and FIC of Ag-RBITC NPs, Ag NPs and vancomycin alone and in combination against VRE and VRE

| | | | MIC (mg $L^{-1}$) | | | | FIC | |
| --- | --- | --- | --- | --- | --- | --- | --- | --- |
| | Ag NPs alone | Ag-RBITC alone | Vancomycin alone | Ag NPs in combination | Ag-RBITC in combination | Vancomycin in combination | Ag-RBITC | Ag NPs |
| VSE | 13.5 | 13.5 | 2 | 1.69 | 1.69 | 1 | 0.63 | 0.63 |
| VRE | 13.5 | 13.5 | 512 | 3.38 | 3.38 | 2 | 0.25 | 0.25 |

This journal is © The Royal Society of Chemistry 2025

*J. Mater. Chem. B*, 2025, **13**, 10903–10915 | **10909**
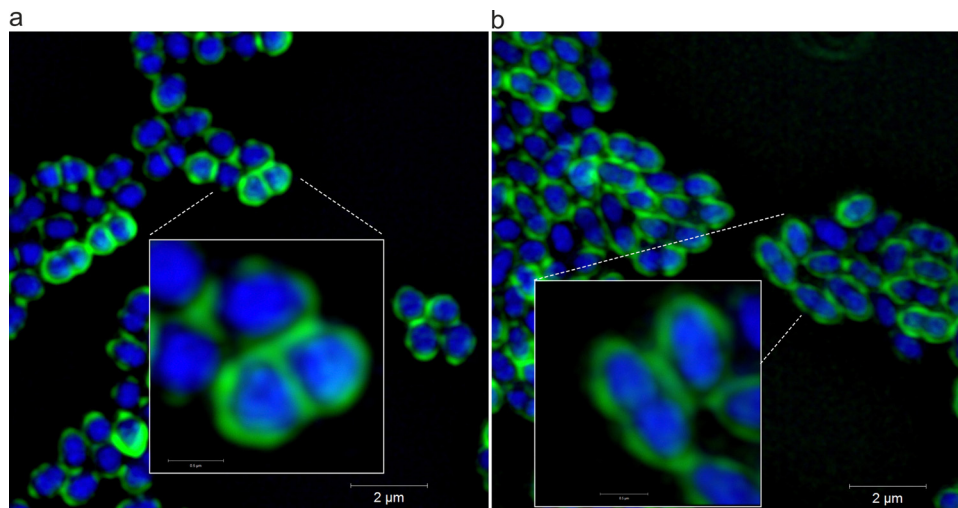
Paper

**Fig. 5**  Fluorescence microscopy images showing the localization of vancomycin in the cell wall and septum of VSE (a) and only in the cell wall of VRE (b) after 15 minutes of incubation with vancomycin.

consisting of a chemical alteration of the target site. The bactericidal mechanism of action of the glycopeptide vancomycin consists in binding to the terminal D-Ala-D-Ala dipeptide of the bacterial peptidoglycan in the cell wall of Gram-positive bacteria. Formation of the glycopeptide–peptidoglycan complex leads to inhibition of cell wall transpeptidase, which maintains the integrity of the wall, thereby stopping cell wall biosynthesis, blocking cell division and bacterial growth.[4] This leads to instability of the cell wall and as a result of the internal osmotic pressure, the bacteria rupture depending on the osmotic conditions around the bacterial cell.[8] However, enterococci can effectively resist this mechanism of action. Vancomycin-resistant enterococci exhibit VanA, VanB or VanD phenotypes that incorporate the depsipeptide D-Ala-D-lactate into the peptidoglycan. This results in the loss of one hydrogen bond in the glycopeptide–lipid II complex and unfavourable proximity of

repulsive carbonyl and ester oxygen atoms, which combine to produce a 1000-fold lower affinity between the glycopeptide and the depsipeptide.[7] Another possible mechanism of bacterial resistance to vancomycin is the formation of false target sites in the cell wall to which vancomycin binds and thus cannot enter the bacterium and block cell wall synthesis in the septum.[6] As a result, in the case of $VRE_{Van}$, vancomycin was localized only in the cell wall and not in the septum, and thus bacterial cell division was not inhibited, and no bactericidal effect was achieved.

**3.3.2.  VSE and VRE bacteria exposed to Ag-RBITC NPs.** After $VSE_{Ag}$ and $VRE_{Ag}$ were exposed to Ag-RBITC NPs at a concentration of 10 mg $L^{-1}$, the Ag NPs penetrated the cell wall of both bacteria and were localized inside the bacteria by fluorescence microscopy (Fig. 6). However, the distribution of Ag-RBITC NPs inside the bacteria was not homogeneous and
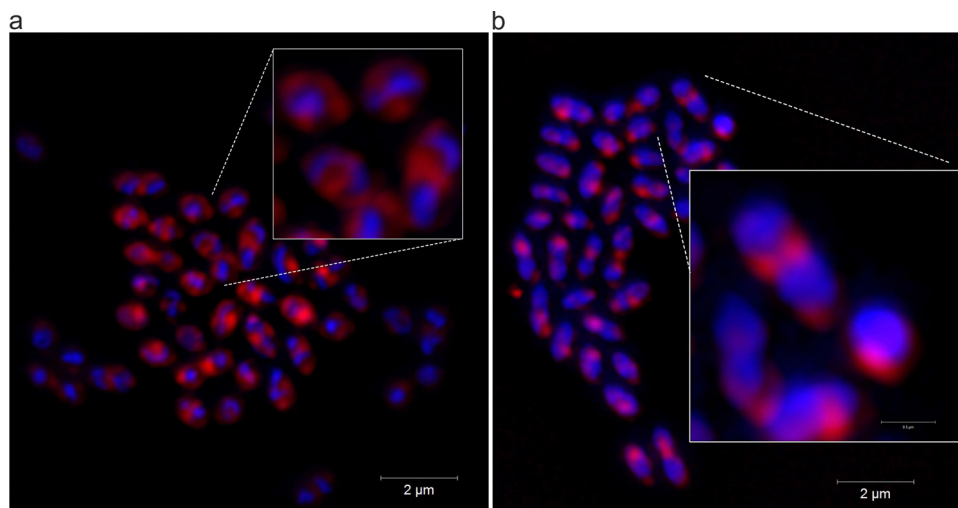


**Fig. 6**  Fluorescence microscopy images showing the localization of Ag-RBITC particles inside $VSE_{Ag}$ (a) and $VRE_{Ag}$ (b) bacteria after 15 minutes of incubation with Ag-RBITC.

differed slightly between the two bacteria. In the case of $VSE_{Ag}$, Ag NPs surrounded the bacterial DNA fairly uniformly (Fig. 6a) and were also likely present in the nascent septum during bacterial division. For $VRE_{Ag}$, the distribution of Ag nanoparticles in the cell appeared to be irregular and more concentrated to a specific location around the DNA (Fig. 6b). A significant difference between bacteria exposed to Ag-RBITC NPs (Fig. 6) and bacteria exposed only to vancomycin without Ag-RBITC particles (Fig. 5) was observed in the shape of DNA at the sites of exposure to Ag NPs. In the case of $VSE_{Ag}$ and $VRE_{Ag}$ bacteria exposed to Ag NPs, there were significant morphological changes in bacterial DNA, probably due to its denaturation or condensation caused by Ag NPs. Inhibition of DNA replication or DNA damage (condensation and deformation) due to silver particles and $Ag^{+}$ cations have been previously confirmed by molecular biology methods,[52–56] but this is the first time that Ag NPs-induced DNA damage in bacteria has been observed directly by fluorescence microscopy. In VRE, although the intracellular distribution of Ag-RBITC appears more localized, the particles still enter the cells, reach critical intracellular sites, and induce DNA condensation and damage, as shown by fluorescence imaging. This is likely sufficient to exert inhibitory bacteriostatic or bactericidal effects, even if the distribution is not uniform. Despite different intracellular localization, the net biological effect at the tested concentrations is comparable, leading to identical MIC values in both strains.

**3.3.3. VSE and VRE bacteria exposed to a combination of vancomycin and Ag-RBITC.** In the case of $VSE_{Van\_Ag}$ and $VRE_{Van\_Ag}$ bacteria exposed to Ag-RBITC NPs in combination with vancomycin, changes were evident between $VSE_{Van\_Ag}$ and $VRE_{Van\_Ag}$, particularly in the damage to the bacterial cell wall, as evident by visualization of the fluorescently labelled vancomycin and its presence in the cell wall and possibly in the septum (only in $VSE_{Van\_Ag}$). Vancomycin was uniformly and significantly distributed in the cell wall and septum in the case of $VSE_{Van\_Ag}$, where Ag NPs were also localized (Fig. 7a). These were also shown to act inside the cell, where they again tightly surrounded the bacterial DNA and again caused damage to the bacterial DNA as in the case of $VSE_{Ag}$ (Fig. 6a). Likewise, in the case of $VRE_{Van\_Ag}$, Ag NPs were also located inside the cell, where they surrounded and deformed the bacterial DNA (Fig. 7b). Vancomycin was very in-homogeneously and unevenly localized in $VRE_{Van\_Ag}$ and only in the cell wall, not in the septum. The images also show that there was significant damage to the bacterial wall, which is very evident in the case of $VRE_{Van\_Ag}$ in Fig. 7b. In a large number of $VRE_{Van\_Ag}$ bacteria, the bacterial wall is partially or completely absent and only the protoplast containing a deformed nucleus surrounded by Ag NPs is shown. The bacterial cell shows significant damage and disruption.

The images of VSE and VRE bacteria shown in Fig. 6 and 7 reveal a noticeable difference in the fluorescence intensity of Ag-RBITC particles, which correlates with the different distribution of Ag NPs in the bacterial cell. However, a more in-depth quantitative comparison and interpretation of different fluorescence intensities is not applicable in this case. This is because the fluorescence intensity of the fluorophore is influenced to a certain extent by the high-resolution SIM technique itself. The reconstruction algorithms and processing steps involved in the SIM technique make it unsuitable for a quantitative comparison of fluorescence signal intensities.

It is evident from the microscopic images that the action of Ag NPs is involved in the deformation and damage of the cell wall in this case. This mechanism of cell damage is typical of Ag nanoparticles and has been observed earlier in many previous works. For example, Woo *et al.* observed cell wall damage in *S. aureus* by TEM, where the action of silver cations resulted in significant disruption of the peptidoglycan cell wall.[57] However, in addition to Ag NPs, vancomycin itself may also be involved in cell wall damage due to the specific mechanism of bacterial resistance to vancomycin. Besides the chemical alteration of
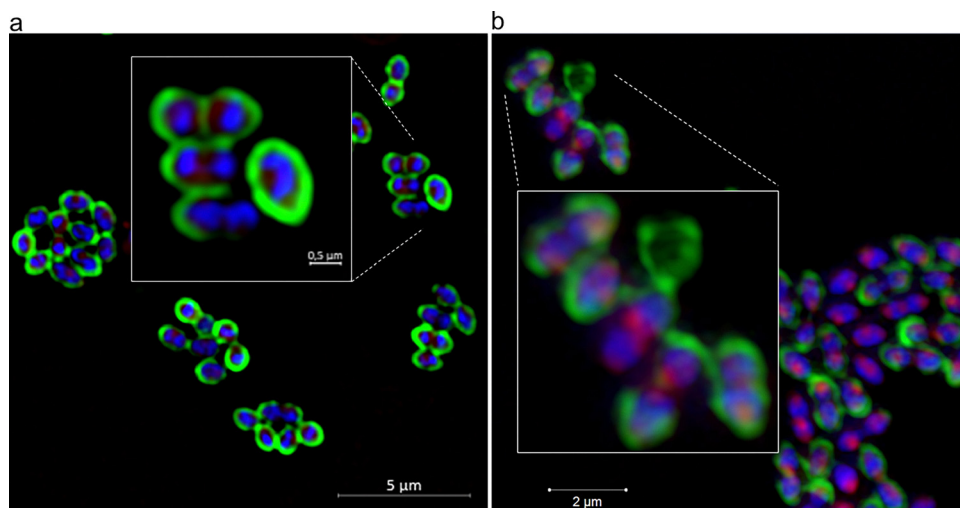


**Fig. 7** Fluorescence microscopy images showing the localization of Ag-RBITC NPs and vancomycin inside $VSE_{Van\_Ag}$ (a) and $VRE_{Van\_Ag}$ (b) bacteria after 15 minutes of incubation with Ag-RBITC NPs in combination with vancomycin.

the antibiotic target site, the resistance of vancomycin-resistant *S. aureus* to vancomycin has previously been explained by the increased tendency of vancomycin to bind to the cell wall. In this particular case, vancomycin molecules primarily bind to the cell wall where the bacteria form false target binding sites, thereby blocking further entry of the antibiotic into the target sites in the septum.[6] Vancomycin-intermediate *S. aureus* strains (VISA strain) have also been shown to have a thickened cell wall that protects ongoing peptidoglycan biosynthesis from the effects of vancomycin. In these cases, abnormal diffusion and concentration of vancomycin into the cell wall occur and the subsequent cooperative effect of plugging and increase in cell wall thickness prevents vancomycin action at the target site in the septum in VISA strains.[10] However, the retention of vancomycin molecules and their concentration in the cell wall may affect its strength and permeability when exposed to Ag NPs, which may result in a greater susceptibility and sensitivity to cell wall damage by their action. When vancomycin is combined with Ag NPs, the cell wall is then more easily disrupted and ruptured in $VRE_{Van\_Ag}$ bacteria, that are more susceptible to Ag NPs than $VSE_{Van\_Ag}$.

In addition, by imaging the bacteria in the confocal mode of the microscope, it was possible to compare vancomycin signal intensities in $VRE_{Van}$ and $VRE_{Van\_Ag}$ bacteria. The images of the bacteria shown in the previous Fig. 5–7 were taken using the super-resolution SIM method, which is not suitable for quantitative comparison of fluorescence signal intensities. When $VRE_{Van}$ exposed to vancomycin alone (Fig. 8a) was imaged in normal confocal mode (not SIM), its intensity was significantly weaker than that of the $VRE_{Van\_Ag}$ sample (Fig. 8b). This clearly indicates that more vancomycin binds to $VRE_{Van\_Ag}$ cell walls in combination with Ag NPs as a result of Ag NPs interacting with cells to affect cell wall permeability and disrupt the cell wall and cytoplasmic membrane. The action of Ag NPs increases the permeability of the bacterial wall, allowing vancomycin molecules to enter the cell wall more easily and quickly, where they then accumulate in higher concentrations.

### 3.4. ROS measurement

One of the mechanisms of action of Ag NPs that contributes to increased permeability and disruption of the cell wall and cytoplasmic membrane is the generation of ROS and subsequent oxidative stress. To confirm this mechanism in the case of this study, ROS production was determined in the presence of VSE and VRE bacteria exposed to Ag NPs at concentrations ranging from 5 mg L$^{-1}$ to 50 mg L$^{-1}$ for 24 h. From the measured data, an increase in ROS production with increasing concentration of Ag NPs was clearly demonstrated (Fig. 9). Statistical analysis of variance (ANOVA) was performed and showed statistically significant differences for both VSE and VRE strains tested after 24 h as a function of Ag NPs concentration ($p < 0.0001$ for both). Using Dunnett's multiple comparison tests (see Table S1), ROS production was compared for all Ag NPs concentrations relative to the control, with significant differences highlighted by an asterisk (Fig. 9). In the case of Ag NPs, significant differences were observed from a concentration of 10 mg L$^{-1}$ against VRE and from 20 mg L$^{-1}$ against VSE. No significant difference with respect to the control was observed at Ag NPs concentrations of 5 mg L$^{-1}$ against VRE and 10 mg L$^{-1}$ against VSE and also in the case of vancomycin alone at a concentration of 1 mg L$^{-1}$. On the contrary, in the combination of 1 mg L$^{-1}$ vancomycin and 10 mg L$^{-1}$ Ag NPs against both VRE and VSE strains, the increase in ROS production was significant, demonstrating the presence of increased ROS production and thus damage to the bacterial cell wall and cytoplasmic membrane when bacteria were exposed to the combination of vancomycin and Ag NPs even at low concentrations of vancomycin, which are ineffective against VRE. The demonstrated oxidative stress induced by ROS produced in the presence of Ag NPs is most likely responsible for the disruption of the cell wall and cytoplasmic membrane of VRE and VSE bacteria and is involved in increasing its permeability and in the synergistic effect of Ag NPs with vancomycin itself. Hydrogen peroxide H$_2$O$_2$ was used as a positive control for ROS generation
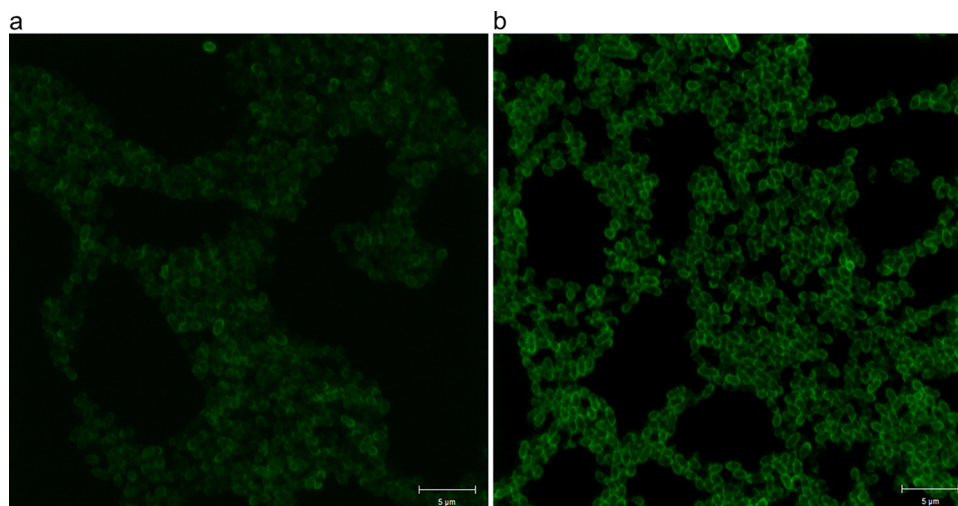


Fig. 8 Comparison of vancomycin signal intensities in VRE using confocal imaging: (a) $VRE_{Van}$ and (b) $VRE_{Van\_Ag}$.
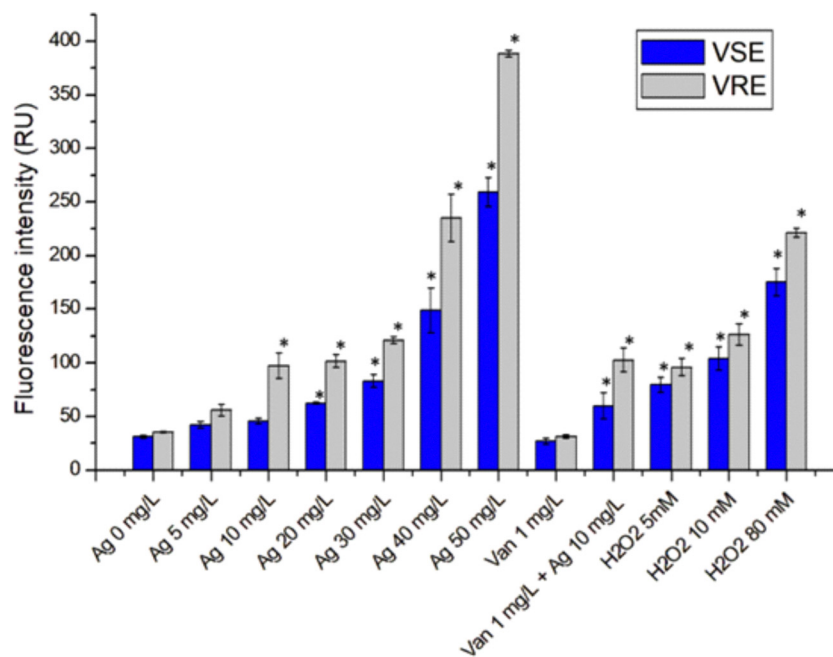
**Fig. 9** Determination of ROS production for VSE and VRE exposed to different concentrations of AgNPs, vancomycin, their combination and $H_2O_2$ as a positive control.

in both cases (with and without bacteria). In the case of negative controls (nanoparticles without bacteria), no significant trend of ROS increase with increasing concentration of Ag NPs was observed (Fig. S2).

## 4. Conclusion

Using fluorescence microscopy, the mechanism of synergistic antibacterial action against vancomycin-susceptible and vancomycin-resistant enterococci was described based on the localization of rhodamine-labelled Ag NPs and the fluorescent vancomycin conjugate BODIPY FL. In the case of vancomycin itself, its localization at the target site in the septum of VSE, where it inhibits cell wall synthesis, was confirmed. In contrast, in the case of VRE, vancomycin was only bound in the cell wall due to resistance consisting in a chemical change of the target site. In the case of the combination of Ag NPs and vancomycin, it has been discovered for the first time by fluorescence microscopy that the synergistic antibacterial effect of vancomycin and Ag NPs is mainly due to the disruption of the permeability and strength of the cell wall. Cell wall becomes very unstable and loses its strength, resulting in its disruption and detachment when bacteria were treated by Ag NPs and vancomycin probably thanks to ROS production by Ag NPs and residual antibacterial effect of vancomycin. In addition, Ag NPs at the same time significantly deform the bacterial DNA, which also contributes significantly to the inhibition of bacterial multiplication and finally to synergistic antibacterial effects. The synergistic effect of Ag NPs with vancomycin is due to the production of ROS and the subsequent oxidative stress induced when Ag NPs are exposed to bacteria. Moreover, in the case of

VRE, vancomycin molecules tend to bind more primarily to false sites in the cell wall, blocking further entry of the antibiotic into the target sites in the septum. The retention of vancomycin molecules and their concentration in the cell wall may affect the strength and permeability of the cell wall, which may result in a greater susceptibility to damage by Ag NPs. In combination with silver, the cell wall of VRE is then disrupted and ruptured, which is likely to be more susceptible to Ag NPs than the VSE. Although the mechanism of the synergy between Ag NPs and vancomycin was not yet fully understood, this study was the first to visualize and localize the distribution of vancomycin together with Ag NPs inside a bacterial cell and thus describe the mechanism of their joint effect based on cell wall disruption and DNA deformation. This work can help to better understand the mechanisms of synergistic effects of Ag NPs with antibiotics against resistant bacteria which represent an important finding for potential approach to an effective fight against the unresolved problem of an increasing resistance of pathogenic bacteria against traditional antibiotics.

## Author contributions

L. V. and L. S. H. – conceptualization, writing – original draft, resources, investigation, visualization and validation. M. M. – investigation, methodology. M. K. – conceptualization, supervision. K. L. formal analysis. H. K. writing – review & editing, methodology. B. S. – resources, methodology. R. P. – resources, methodology. L. K. – methodology, writing – review & editing. A. P. – conceptualization, writing – review & editing, project administration, supervision.

This journal is © The Royal Society of Chemistry 2025

*J. Mater. Chem. B*, 2025, **13**, 10903–10915 | **10913**

## Conflicts of interest

There are no conflicts to declare.

## Data availability

All data needed to evaluate the conclusions in the paper are present in the paper and/or the SI. Supplementary Information file content: Experimental details (chemicals and biological materials), full MTT cytotoxicity protocol on HaCaT keratinocytes, statistical analysis with full Dunnett's results (Table S1), Fig. S1 (HaCaT viability) and Fig. S2 (ROS negative controls). See DOI: https://doi.org/10.1039/d5tb01231g

Additional data related to this paper may be requested from the authors.

## References

1 I. Sultan, et al., Front. Microbiol., 2018, 9, DOI: 10.3389/fmicb.2018.02066.
2 Y. Cetinkaya, P. Falk and C. G. Mayhall, Clin. Microbiol. Rev., 2000, 13, 686–707.
3 M. O. Ahmed and K. E. Baptiste, Microb. Drug Resist., 2018, 24, 590–606.
4 J. C. J. Barna and D. H. Williams, Annu. Rev. Microbiol., 1984, 38, 339–357.
5 M. G. Pinho and J. Errington, Mol. Microbiol., 2003, 50, 871–881.
6 P. M. Pereira, et al., Antimicrob. Agents Chemother., 2007, 51, 3627–3633.
7 G. D. Wright, Curr. Opin. Chem. Biol., 2003, 7, 563–569.
8 P. Hildebrandt, et al., Cytometry, Part A, 2016, 89, 932–940.
9 G. Li, M. J. Walker and D. M. P. De Oliveira, Microorganisms, 2023, 11, DOI: 10.3390/microorganisms11010024.
10 L. Cui, et al., Antimicrob. Agents Chemother., 2006, 50, 428–438.
11 A. Panáček, et al., Colloids Surf., B, 2016, 142, 392–399.
12 A. Panácek, et al., Molecules, 2016, 21, 1–17.
13 T. Bruna, et al., Int. J. Mol. Sci., 2021, 22, 7202.
14 S. Prabhu and E. K. Poulose, Int. Nano Lett., 2012, 2, 32–41.
15 T. C. Dakal, et al., Front. Microbiol., 2016, 7, DOI: 10.3389/fmicb.2016.01831.
16 M. A. Quinteros, et al., Toxicol. Vitro, 2016, 36, 216–223.
17 L. Hochvaldová, et al., Sci. Rep., 2022, 12, DOI: 10.1038/s41598-022-09294-7.
18 L. Hochvaldová, et al., Nanotechnol. Rev., 2022, 11, 1115–1142.
19 I.-S. Hwang, et al., J. Med. Microbiol., 2012, 61, 1719–1726.
20 R. Vazquez-Muñoz, et al., PLoS One, 2019, 14, DOI: 10.1371/journal.pone.0224904.
21 N. S. Swidan, et al., Sci. Rep., 2022, 12, DOI: 10.1038/s41598-022-07831-y.
22 D. Sharma, L. Misba and A. U. Khan, Antimicrob. Resist. Infect. Control, 2019, 8, DOI: 10.1186/s13756-019-0533-3.
23 H. Deng, et al., Environ. Sci. Technol., 2017, 50, DOI: 10.1038/srep46687.
24 S. Ghosh, et al., Int. J. Nanomed., 2012, 7, 483–496.
25 A. I. Ribeiro, A. M. Dias and A. Zille, ACS Appl. Nano Mater., 2022, 5, 3030–3064.
26 A. Kaur, et al., Colloids Surf., B, 2019, 176, 62–69.
27 M. Awad, et al., Biol. Trace Elem. Res., 2021, 199, 4225–4236.
28 M. Esmaeillou, et al., Adv. Pharm. Bull., 2017, 7, 479–483.
29 K. Morimoto, et al., PLoS One, 2014, 9, 1–8.
30 K. T. Hassan, et al., J. Environ. Chem. Eng., 2021, 9, DOI: 10.1016/j.jece.2021.105359.
31 P. Lin, Z.-F. Yan and C.-T. Li, Biotechnol. Bioprocess Eng., 2021, 26, 650–659.
32 H. R. Ali, et al., J. Nanopart. Res., 2021, 23, DOI: 10.1007/s11051-021-05349-4.
33 N. Ilahi, et al., Microsc. Res. Tech., 2022, 85, 1568–1579.
34 Y. Sheng, et al., Process Biochem., 2022, 112, 241–247.
35 K. Khleifat, et al., J. Pure Appl. Microbiol., 2022, 16, 1722–1735.
36 A. M. Alotaibi, et al., Antibiotics, 2022, 11, DOI: 10.3390/antibiotics11091219.
37 P. R. More, et al., Pharmaceutics, 2022, 14, 2457, DOI: 10.3390/pharmaceutics14112457.
38 Y. Yan, et al., Adv. Healthcare Mater., 2023, 12, DOI: 10.1002/adhm.202301157.
39 A. J. Munoz, et al., World J. Microbiol. Biotechnol., 2023, 40, DOI: 10.1007/s11274-023-03825-8.
40 K. Patel and R. Kumar, ChemistrySelect, 2020, 5, 4701–4707.
41 S. Masoumi, et al., Arch. Pediatr. Infect. Dis., 2018, 6, DOI: 10.5812/pedinfect.57920.
42 S. R. Sarhan and O. M. S. Ibrahim, Adv. Anim. Vet. Sci., 2018, 6, 2307–8316.
43 M. Carrizales, et al., Antibiotics, 2018, 7, DOI: 10.3390/antibiotics7020050.
44 D. Lin-Vien, et al., Alkanes, in The Handbook of Infrared and Raman Characteristic Frequencies of Organic Molecules, ed. D. Lin-Vien, et al., Academic Press, San Diego, 1991, ch. 2, pp. 9–28.
45 D. Lin-Vien, et al., Aromatic and Heteroaromatic Rings, in The Handbook of Infrared and Raman Characteristic Frequencies of Organic Molecules, ed. D. Lin-Vien, et al., Academic Press, San Diego, 1991, ch. 17, pp. 277–306.
46 D. Lin-Vien, et al., Double Bonds Containing Nitrogen Atoms, in The Handbook of Infrared and Raman Characteristic Frequencies of Organic Molecules, ed. D. Lin-Vien, et al., Academic Press, San Diego, 1991, ch. 12, pp. 191–211.
47 D. Lin-Vien, et al., Compounds Containing the Carbonyl Group, in The Handbook of Infrared and Raman Characteristic Frequencies of Organic Molecules, ed. D. Lin-Vien, et al., Academic Press, San Diego, 1991, ch. 9, pp. 117–154.
48 D. Lin-Vien, et al., The −C≢N and −N≢C Groups, in The Handbook of Infrared and Raman Characteristic Frequencies of

10914 | J. Mater. Chem. B, 2025, 13, 10903–10915

This journal is © The Royal Society of Chemistry 2025

*Organic Molecules*, ed. D. Lin-Vien, *et al.*, Academic Press, San Diego, 1991, ch. 8, pp. 105–115.

49 D. Lin-Vien, *et al.*, Compounds Containing –NH2, –NHR, and –NR2 Groups, in *The Handbook of Infrared and Raman Characteristic Frequencies of Organic Molecules*, ed. D. Lin-Vien, *et al.*, Academic Press, San Diego, 1991, ch. 10, pp. 155–178.

50 D. Lin-Vien, *et al.*, Alkenes, in *The Handbook of Infrared and Raman Characteristic Frequencies of Organic Molecules*, ed. D. Lin-Vien, *et al.*, Academic Press, San Diego, 1991, ch. 6, pp. 73–94.

51 A. Panáček, *et al.*, *Molecules*, 2016, **21**(26), DOI: **10.3390/molecules21010026**.

52 Q. L. Feng, *et al.*, *J. Biomed. Mater. Res.*, 2000, **52**, 662–668.

53 Y. Dong, *et al.*, *PLoS One*, 2019, **14**, 1–12.

54 S. Nallanthighal, *et al.*, *NanoImpact*, 2020, **17**, 100205.

55 H. S. Jiang, *et al.*, *Small*, 2019, **15**(27), DOI: **10.1002/smll.201900860**.

56 L. Zou, *et al.*, *Sci. Rep.*, 2018, **8**, DOI: **10.1038/s41598-018-29313-w**.

57 K. J. Woo, *et al.*, *Appl. Environ. Microbiol.*, 2008, **74**, 2171–2178.

This journal is © The Royal Society of Chemistry 2025

*J. Mater. Chem. B*, 2025, **13**, 10903–10915 | **10915**